Journal of Materials Chemistry A

Accepted Manuscript

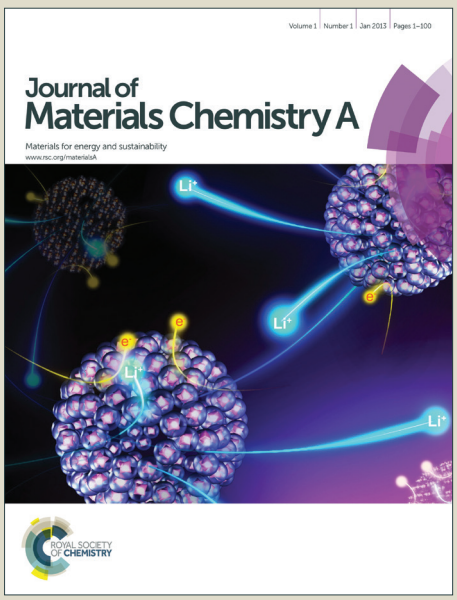

ROYAL SOCIETY OF CHEMISTRY

www.rsc.org/materialsA

Armored Cobalt-Citrate Framework with Graphene Oxide Exhibiting Improved Thermal Stability and Selectivity for Biogas Decarburization

Yangcan Shen,[1,2] Ziyin Li,[1] Lihua Wang,[1] Yingxiang Ye,[1] Qing Liu,[1] Xiuling Ma,[1] Qianhou Chen,[1] Zhangjing Zhang[1,*] and Shengchang Xiang[1,3,*]

[1] *Fujian Provincial Key Laboratory of Polymer Materials, College of Material Sciences and Engineering, Fujian Normal University, 32 Shangsan Road, Fuzhou 350007,China*

Corresponding Author E-mails: Z. Zhang (zzhang@fjnu.edu.cn) and S. Xiang (scxiang@fjnu.edu.cn)

[2] *State Key Laboratory of Structural Chemistry, Fujian Institute of Research on the Structure of Matter, Chinese Academy of Sciences, Fuzhou, Fujian 350002, PR China*

[3] *College of Life and Environmental Sciences, Minzu University of China, 27 South Zhongguancun Boulevard, Haidian District, Beijing 100081, China*

Abstract

A serial of metal-organic frameworks (UTSA-16)–graphene oxide (GO) composites were synthesized, which is the first example of core-shell type MOF composite armored with GO film. The parent materials (UTSA-16 and GO) and the nanocomposite were characterized using X-ray diffraction, SEM, TEM, TGA and gas adsorption, which show up a greatly improved thermal stability. At the same time, UTSA-16-GO19 has the CO_2/CH_4 selectivity of 114.4, which is three times more than that for UTSA-16 and only lower than polyamine incorporated amine-MIL-101(Cr) among the reported MOFs materials. The GO composites provide a new direction for making practical MOF materials with high performance.

1. Introduction

Because of the limitations in energy from fossil oil resources and the constant increase of world energy needs, much attentions have been paid to renewable and environmentally friendly energy sources in both developed and developing countries nowadays. Biogas is one of the most promising candidates for the energy power solution with its environmental and economical attraction. As of 2012 Europe has already over 13800 biogas plants and more than 7400 MW_{el} of installed capacity.[1] Since 2006 Renewable Energy Law came into operation in China, the biogas industry has been growing fast, the annual amount reaching of 15.5 billion m^3 in 2011.[2] It is pity that, apart from main component methane, biogas often contains significant amounts of CO_2 (20−45 vol%), with some water vapor, H_2S, and other minor impurities. Due to the low quality, the use of biogas is limited mainly in rural household heating and electricity, despite of the low energy utilization efficiency. The unsmooth market circulation leads to excess generating capacity for the regional biogas. Some rural plants have to release part of gaseous fuels to avoid the overflow of biogas slurry. It has been realized that the selective removal of CO_2 for biogas updating to biomethane is important and urgent for both environmental and economic reasons. In view of environmental regulations, methane is the most important non-CO_2 greenhouse gas (GHG), accounting for 10% of total GHG emissions in developed countries and almost 20% in developing countries.[3] The greenhouse warming potential of methane is 21 times higher and the lifetime of methane molecules in the atmosphere is 10 times longer than CO_2 molecules. On the other hand, the presence of CO_2 reduces its energy content and leads to the corrosion of biogas pipelines. Prior to pipeline transportation, CO_2 should be removed to meet the typical specification on CO_2 of 3%.

Current technologies for biogas upgrading are often multi-stage processes to remove the impurities, and thus costly. Beyond the state-of-the-art amine-scrubbing technology for acid gas removal suffering from high energy penalty for the solvent regeneration,[4] physical adsorption over porous solids provides alternative to the easy-on and easy-off carbon capture and separation.[5-18] Among the porous solids,[19-29] spurred enthusiasm for crystalline microporous metal-organic frameworks (MOFs) working as carbon capture materials has spread quickly,[30-41] because their designable framework structures, crystallinity and high surface areas provide great opportunities to enable diffraction experiments to uncover specific binding sites for CO_2 in pores, as well as to systemically modify adsorption capacity, enthalpy and selectivity toward CO_2. It is worth noting that the poor resistibility to heat, water and chemicals is widely considered to be a major weakness of MOFs that could negate potential advantages of the MOFs materials from an applications perspective. Recently, a new tendency to hybrid the MOFs with various species has emerged, resulting in the composites with an improved performance unattainable by the individual constituents for carbon capture.[42] Such species include metal nanoparticles/nanorods, oxides, quantum dots, polyoxometalates, polymers, graphene and graphene oxide (GO), carbon nanotubes and biomolecules. After the pioneered work reported by T. J. Bandosz,[43-47] the GO composites based on some MOFs, including MOF-5,[43,44,48] MIL-100(Fe),[45] HKUST-1[46,47,49,50] and MIL-101(Cr),[51] have been synthesized by simply dispersing GO powder into the MOF synthesis mixtures. In all cases above, grapheme oxide constituents are highly dispersed in the composites and no core-shell type is observed. Although the MOF-GO composites show great resistibility to the toxic gases and can be developed as their potential storage media, but the researches on biogas purity have not been studied. Only the HKUST-1 composite has been demonstrated a higher capacity of CO_2 at 1 atm and 273 K.[49]

In our previous work, UTSA-16 with diamondoid cages are promising in the carbon capture, showing low adsorption enthalpy (34 kJ/mol) and high capacity for CO_2 due to the synergistic effect of the weak adsorbent-adsorbate interactions.[40] However, it is still challenge for UTSA-16 to be used in industrial world because its poor thermal stability with collapse temperature at 139 ^oC as well as its relatively low selectivity (29.8) for equimolar CO_2/CH_4 mixture. Inspired the speculation that the carboxylate O atoms on the surface of UTSA-16 may interact with the plentiful –OH and carboxyl groups of GO to produce the composites with novel performance (scheme 1), we synthesized and then characterized a serial of hybridized UTSA-16-GO composites with various GO contents. Their features, including the morphology, selective adsorption and thermal stability, are compared with the parent materials.

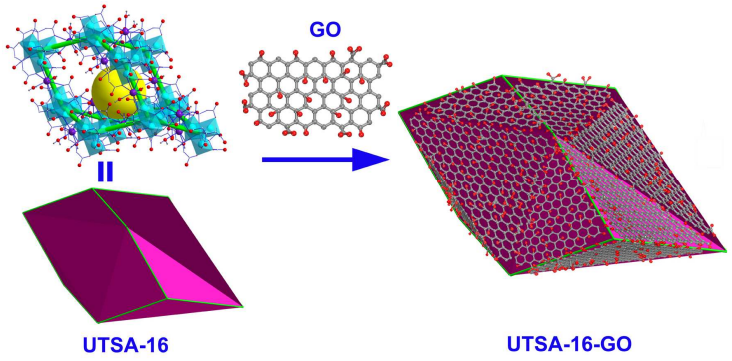

Scheme 1. A schematic diagram showing the formation of the UTSA-16-GO composites

2. Experiment section

2.1 Materials and Characterization

All reagents and solvents used in synthetic studies were commercially available and used as supplied without further purification. X-ray powder diffraction data were recorded on a Rigaku MultiFlex diffractometer at 40 kV,

40 mA for Cu Kα (λ = 1.5406 Å), with a scan speed of 10 deg/min. A Micromeritics ASAP 2020 surface area analyzer was used to measure gas adsorption. The sorption measurement was maintained at 77 K with liquid nitrogen and at 273 K with an ice-water bath (slush), respectively. A water bath was used for adsorption isotherms at 296 K. The FTIR (KBr pellets) spectra were recorded in the range of 500～4000 cm^{-1} on a Thermo Nicolet 5700 FT-IR instruments. Thermal analysis was carried out on a METTLER TGA/ SDTA 851 thermal analyzer from 30 to 600 °C at a heating rate of 10 °C/min under nitrogen atmosphere. The surface morphology of the samples was observed by using a JSM-7500F (Japan) scanning electron microscope (SEM) after gold deposition. The morphologies of sample were studied using a JEOL-2010 transmission electron microscope (TEM) working at 200 KV. The samples were prepared by placing a drop of product in ethanol onto a continuous carbon-coated copper TEM grid.

2.2 Syntheses

UTSA-16 was prepared by hydrothermal reaction,[52] which is carried out in teflon-lined 23 ml Parr acid digestion bomb. $Co(Ac)_2 \cdot 4H_2O$ (0.249 g 1 mmol), $C_6H_8O_7 \cdot H_2O$ (0.21 g, 1 mmol), KOH (0.168 g, 3 mmol), H_2O (2.5 ml) and C_2H_5OH (2.5 ml) in molar ratio 1:1:3:139:43 are placed in the bomb. The bomb is then placed in a furnace that is heated from room temperature to 120 °C in half an hour, kept at 120 °C for 2 days, and then slowly cooled to room temperature at a rate of 4 °C/h. And violet prismatic crystals UTSA-16 are obtained which were filtered, washed with Et_2O and dried at room temperature.

GO was synthesized by a modified Hummer's method.[53] Briefly, The mixture of graphite powder (3.0 g , synthetic, 1-2 micron and 30 micron) and $NaNO_3$ (1.5 g) is stirred with cold concentrated sulfuric acid (69 ml at 0 °C) in an ice bath for 30 min. Then, potassium permanganate (9.0 g) is added slowly to the suspension to prevent a rapid rise in temperature (less than 20 °C), then, the mixture is stirred for 120 min below 20 °C。The reaction was warmed to 35 °C and stirred for 60 min. Distilled water (138 ml) is slowly added to the reaction vessel to keep the temperature under 98 °C. External heating was introduced to maintain the reaction temperature at 98 °C for 15 min, then the heat was removed and further diluted with distilled water (420 ml), before adding hydrogen peroxide (10 ml). The mixture is left overnight and washed with diluted hydrochloric acid (5%). Graphene oxide particles are separated from the excess liquid by centrifugation and washed with distilled water before it is then freeze-dried to remove water. A fine brown powder of the initial GO was obtained.

The composite materials UTSA-16-GO was prepared by using a similar method employed in synthesis of UTSA-16. The GO powder (9.5, 19 and 28.5 mg) is dispersed in reactant mixture of $Co(Ac)_2 \cdot 4H_2O$, $C_6H_8O_7 \cdot H_2O$, KOH, H_2O and C_2H_5OH with the same doses of all reagents with that of synthesis of UTSA-16. The resulting suspensions were subsequently sonicated sufficiently and subjected to the same synthesis procedure as for UTSA-16. The synthesized composites are referred to as UTSA-16-GO9.5, UTSA-16-GO19 and UTSA-16-GO28.5, respectively.

2.3 Virial Equation Analysis

The virial equation can be written[54,55] as follows:

$$\ln(\frac{n}{p}) = A_0 + A_1 n + A_2 n^2 + \ldots \quad (1),$$

where n is the amount adsorbed (mol g^{-1}) at pressure p (Pa). At low surface coverage, the A_2 and higher terms can be neglected and the equation becomes

$$\ln(\frac{n}{p}) = A_0 + A_1 n \quad (2).$$

A linear graph of $ln(n/p)$ versus n is obtained at low surface coverage and this is consistent with neglecting higher terms in equation (2). A_0 is related to adsorbate-adsorbent interactions, whereas A_1 describes adsorbate-adsorbate interactions. The Virial parameters are given in Table S1.

2.4 Enthalpies of Adsorption

Zero Surface Coverage. The isosteric enthalpies of adsorption at zero surface c over age (Q_{st}, n =0) are a fundamental measure of adsorbate−adsorbent interactions, and these values were obtained from the A_0 values obtained by extrapolation of the virial graph to zero surface coverage.

Van't Hoff Isochore The isosteric enthalpies of adsorption as a function of surface coverage were calculated from the isotherms using the van't Hoff isochore, which is given by the following equation,

$$\ln(p) = -\frac{\Delta H}{RT} + \frac{\Delta S}{R} \quad (3).$$

A graph of *lnP* versus *1/T* at constant amount adsorbed (*n*) allows the isosteric enthalpy and entropy of adsorption to be determined. The pressure values for a specific amount adsorbed were calculated from the adsorption isotherms by the following methods: 1) assuming a linear relationship between adjacent isotherm points starting from the first isotherm point, 2) using the virial equation at low surface coverage. The agreement between the two methods is shown in Figures S12~S14 for the three composites.

2.5 Prediction of the Gas Adsorption Selectivity by IAST

The experimentally measured excess isotherm loadings on pure component isotherms for CO_2, CH_4 at 273K and 296K in materials are converted to absolute loadings using

$$q^{abs} = q^{excess} + pV_{pore} / ZRT \quad (4),$$

where Z is the compressibility factor. The Peng-Robinson equation of state was used to estimate Z. The accessible pore volume within the materials, V_{pore}, is taken to be equal to experimentally determined value.

IAST (ideal adsorption solution theory)[56] was used to predict binary mixture adsorption from the experimental pure-gas isotherms. In order to perform the integrations required by IAST, the single-component isotherms should be fitted by a proper model. In practice, several methods to do so are available. We found for this set of data the single-site Langmuir-Freundlich equation was successful in fitting the data.

$$N = N^{\max} \times \frac{bP^{1/n}}{1 + bP^{1/n}} \quad (5)$$

Here, P is the pressure of the bulk gas at equilibrium with the adsorbed phase (kPa), N is the adsorbed amount per mass of adsorbent (mmol/g), N^{max} is the saturation capacities of sites 1 (mmol/g), b is the affinity coefficients of sites 1 (1/kPa), and n represents the deviations from an ideal homogeneous surface. The fitted parameters were then used to predict multi-component adsorption with IAST. The selectivity $S_{A/B}$ in a binary mixture of components A and B is defined as $S_{A/B} = (x_A/y_A)/(x_B/y_B)$, where x_i and y_i are the mole fractions of component i (i = A, B) in the adsorbed and bulk phases, respectively.

3. Results and discussion

3.1 Preparation. The composite materials are prepared by dispersing various amounts of GO powder into the mixture of $Co(Ac)_2 \cdot 4H_2O$, citrate, KOH, H_2O and C_2H_5OH under the hydro(solvo)thermal reaction. Both citrate and GO contain abundant hydroxyl and carboxyl groups. The conformational flexibility of citrates promotes to chelate cobalt and potassium ions to form the MOF cores before GO wrapping. As reported in our previous work,[40] UTSA-16 is a three-dimensional framework supported by infinite three-dimensional heteronuclear M-O-M connections. There are four crystallographically-dependent terminal water molecules within each of its diamondoid cage of 4.5 Å in diameter. Interestingly, there are plentiful carboxylate O atoms on the surface of UTSA-16 framework, which will interact with –OH and –COOH groups on GO to form O-H···O hydrogen bonding interaction to support the growth of GO shell.

3.2 Morphology and powder diffraction

The core-shell type MOF composite armored with GO film may be achieved, which has been confirmed by the surface morphology of the samples shown in SEM and TEM micrographs (Figure 1). It can be seen from

Figure 1(a) that the synthesized GO materials look like seriously corrugated sheets, which tightly stacked together as a result of dispersive forces and strong specific interactions between the surface groups on the graphene-like layers. The SEM and TEM micrographs of UTSA-16 present the unique and well-defined polyhedron crystals (Figures 1b & S3). After hybridization, UTSA-16-GO19 composites (Figures 1c & 1d) keep the original crystal shape, meanwhile, the crinkled GO films un-uniformly cover on the surface of MOF crystals to produce core-shell type composites. The same texture of the composite with the MOF precursor is also visible in TEM micrographs. As shown in Figures 1e and 1f, the edges of composites are surrounded by the filmy GO sheets. These suggest that the GO sheets are dispersed and conjunct to MOFs in nanoscale level, and the growth and wrap of GO sheets on the surface of MOFs do not destroy the crystalline of MOFs. The "core-shell" structural character for the UTSA-16-GO19 composite with the border GO shell and smaller UTSA-16 core is further confirmed by the HAADF-STEM image and EDS element mapping images (Figure 2). EDS mapping images reveal the different distribution of elements C, O, K and Co in the particle, the distribution C and O are more border than that of K and Co, which is in agree with the EDS line scanning profiles. It is the first example of core-shell like MOFs composites observed with GO. The armor with GO may bring better performance to the composite.

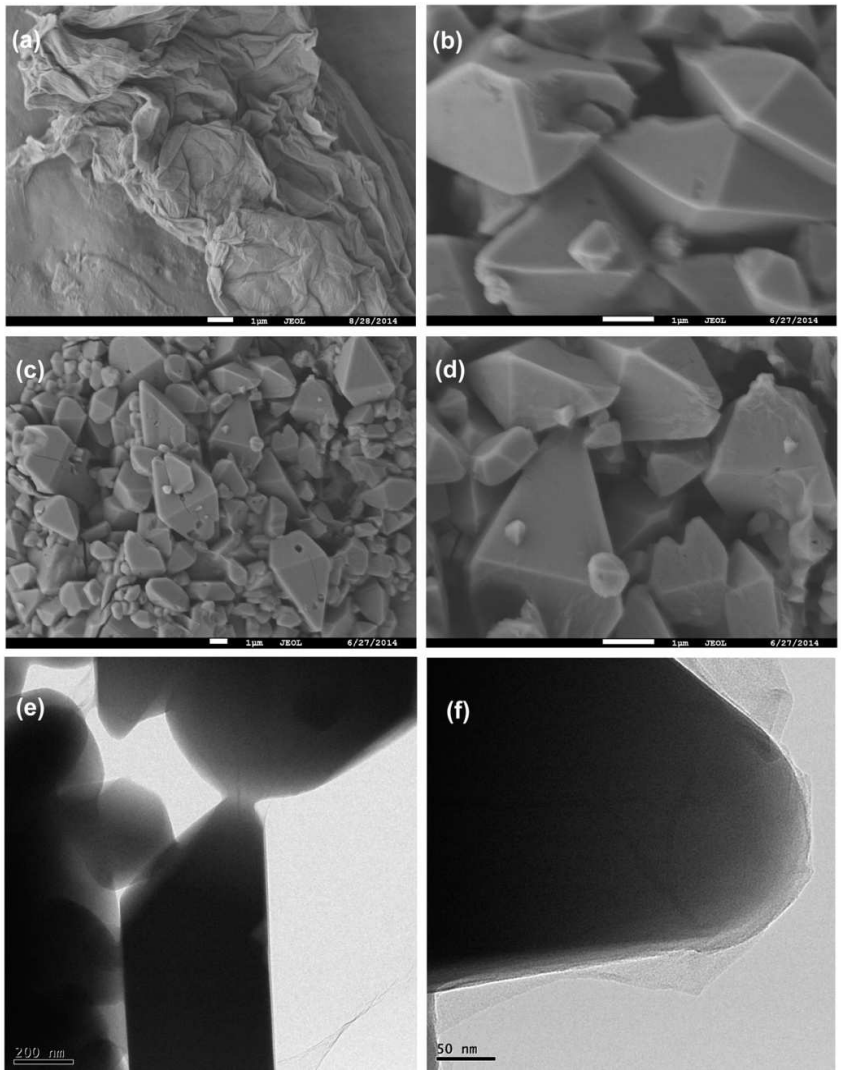

Figure 1. SEM images for GO (a), UTSA-16 (b) and the composite UTSA-16-GO19 (c, d). TEM images for the composite (e) and (f).

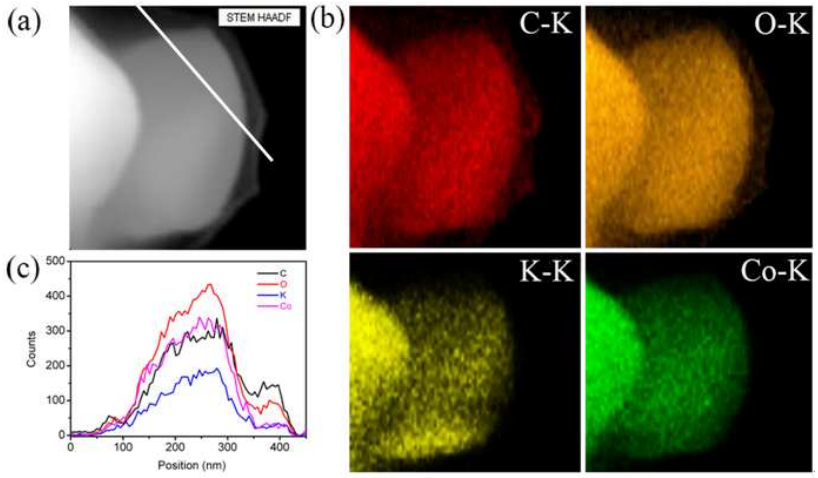

Figure 2. (a) HAADF-STEM image of UTSA-16-GO19 composite with core-shell structure. (b) EDS C-K (red), O-K (orange), K-K (yellow), Co-K (green) mapping images of a single particle, and (c) EDS line scanning profiles as labeled in (a).

The hybrid is further confirmed by the X-ray diffraction patterns of the composites UTSA-16-GO9.5, UTSA-16-GO19 and UTSA-16-GO28.5 as well as their parent materials, as shown in Figure 3. The similar diffraction patterns of the composites to UTSA-16 indicate the existence of the well-defined MOF units, which thus proves that GO did not prevent the formation of linkages between cobalt cations and citrate. A single peak around 2θ of 12.2º for GO reveals a distance between the carbon layers of 7.2 Å, as determined by Bragg's law. But a new peak of 12.4º is observed in the composites, corresponding to GO lattice. The right shift of the GO peak indicates that the GO sheets are incompletely peeled off, although the distance between the carbon layers reduces to 7.1 Å during the composites with UTSA-16.

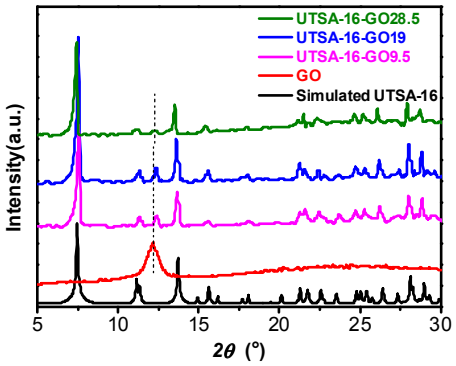

Figure 3. X-ray diffraction pa1tterns of the parent materials and the composites.

3.3 Thermal stability

The thermogravimetry enables to monitor the mass loss as a function of temperature and the curves of UTSA-16, GO and their composites analyzed by heating under N_2 atmosphere from room temperature to 600 ^oC at a rate of 10 ^oC min^{-1} are shown in Figure 4a. For the parent GO, significant weight loss before 120 ^oC is observed, likely due to evaporation of trapped water. In agreement with previous reports,[57] GO is thermally unstable and suffers rapid mass loss upon heating to about 200 ^oC. For UTSA-16, it will gradually lose its mass upon heating to 100 ^oC following with the decomposition and collapse upon 139 ^oC. For the composites, after the removal of solvents between 100~139 ^oC, they can keep their mass up to 340 ^oC followed with the sharp decrease,

corresponding to the decomposition of the frameworks. Obviously, the composites, particularly UTSA-16-GO19, have the higher decomposition and collapse temperature than their parent materials.

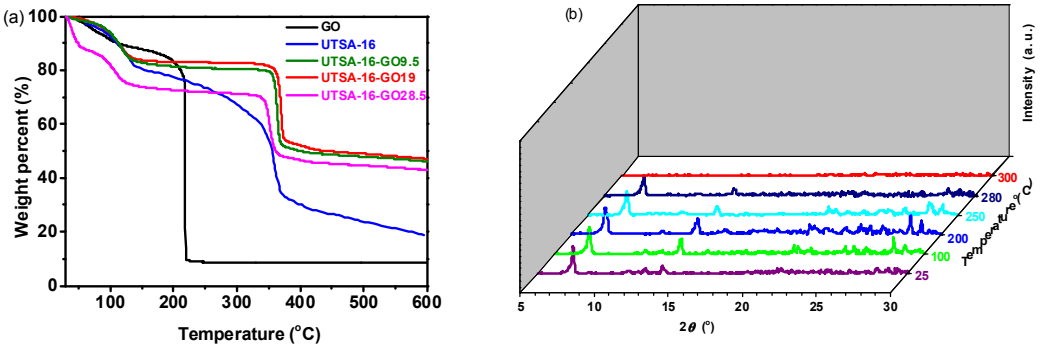

Figure 4. (a) Thermogravimetry analysis of as-synthesized UTSA-16, GO, UTSA-16-GO9.5, UTSA-16-GO19 and UTSA-16-GO28.5. (b) Variable temperature PXRD patterns for UTSA-16-GO19.

It is well-known that TGA is based solely upon combustion of the sample and cannot take into consideration the crystallinity or porosity of the system. TGA studies may not provide the entire picture when investigating thermal stability of porous materials. In-situ variable-temperature PXRD studies, allowing for the observation of the crystallinity of the structure and confirmation of the porous structure, are further employed to evaluate the thermal stability for the representative composite UTSA-16-GO19 in Figure 4b. UTSA-16-GO19 can keep its crystallinity unchanged up to 280 ^{o}C. In agreement with the results from the thermogravimetry analysis, the composite shows higher thermal stability than its parent components. Above 300 ^{o}C, and the composite is destroyed and lose its crystallinity. UTSA-16-GO composites present the first examples reported with the enhancing thermal stability by the GO hybrid approach. The explanation for such reversal in thermal stability may be considered that the existence of strong interactions between GO and MOF framework reinforce the stability of the composite, and the armor of GO films allows for less disruptive movements in the crystal structure with the input of thermal energy, leading to the robust of the crystalline framework. Additionally, the improving thermal stability of the composites may partly be contributed to the increasing thermal conductivity resulted from the graphene introduction.[58] It is worthy to note that there is still rare report to improve the thermal stability of the MOFs materials by the composite approach, although the thermal stability is one of great concerns to their practical applications.

3.4 Gas adsorption

In order to demonstrate the effect of GO armor on the gas adsorption of the composites, N_2 adsorption measurements at 77 K were carried out, and the isotherms are plotted in Figure 5. All the composites display a type I isotherm, indicating the predominant microporous character. With the GO amount added from 9.5 mg, 19 mg to 28.5 mg, the BET surface areas for these composites are of 325, 529 and 487 m^2/g, respectively, all smaller than that of 628 m^2/g for UTSA-16. The GO addition decreases the surface area and pore volume of the composites, but the decrease is not linearly occurred, which is also observed in most of MOF-GO composites reported.[43,48-50] UTSA-16-GO19 with the moderate GO amount has the highest BET surface area among the composites. We thus examined its potential application on the gas selective separation. The adsorption of CO_2 and CH_4 on the composites at 296 K and 273 K are investigated. As shown in Figs. 5b and 5c, the composites can take up differential amount of CO_2 and CH_4, meaning that the selectivities of CO_2/CH_4 can be adjusted via altering their GO amounts. UTSA-16-GO19 can adsorb CO_2 (81 cm^3/g) and CH_4 (11 cm^3/g) at 296 K and 1 atm, slightly lower than the respective values of 96 cm^3/g (CO_2) and 12 cm^3/g (CH_4) for UTSA-16. The well-known ideal adsorbed solution theory (IAST) is employed to evaluate the CO_2/CH_4 separation selectivities on the three

composites for CO_2 capture and separation from equimolar CO_2/CH_4 mixtures and maintained at isothermal conditions at 296 K and pressures up to 200 kPa, as shown in Figure 5d. The separation selectivity on the UTSA-16 composites can be significantly improved due to the GO armor. UTSA-16-GO19 shows the CO_2/CH_4selectivity of 114.4, three times more than that for the parent UTSA-16, higher than the one (105) for Mg-MOF-74,[40,59] and only lower than the ones (278 and 931) for two polyamine-decorated amine-MIL-101 (Cr) materials[60] among the reported MOFs (Table S2). As calculated based on virial method, a well established and reliable methodology from fits of their adsorption isotherms at 273 and 296 K,[54,55] the adsorption enthalpies of UTSA-16-GO19 to CO_2 and CH_4 gases at low coverage are of 42.1 and 11.7 kJ/mol (Table S1), respectively, both higher than the corresponding values for UTSA-16.[40] The enhanced selectivity may be in virtue of the increasing adsorption potential resulted from the GO coverage on the core-shell composites.

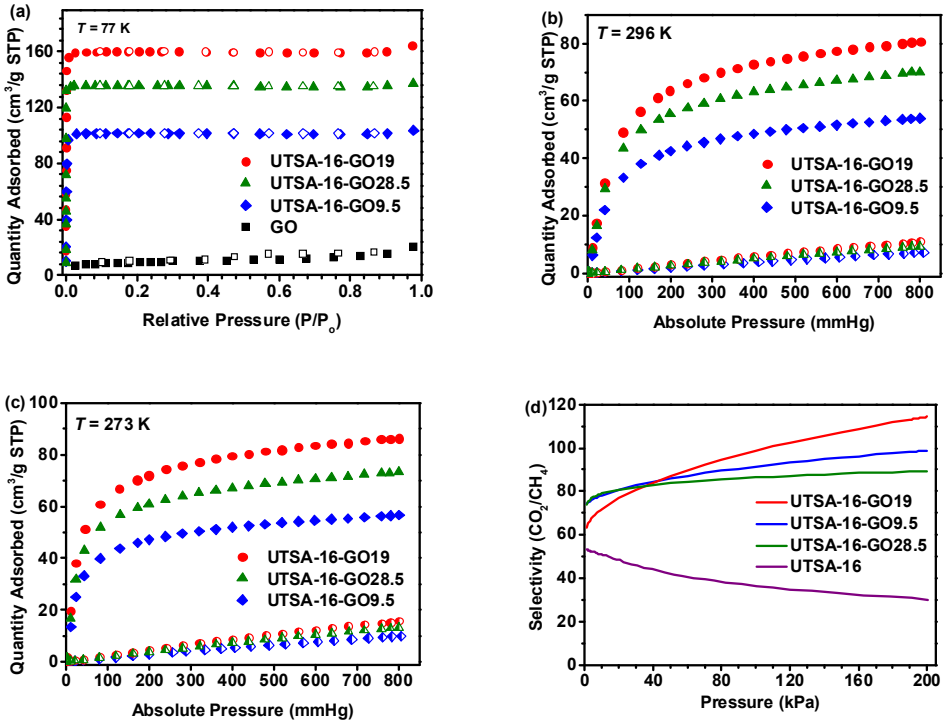

Figure 5. (a) N_2 adsorption isotherms of GO and the UTSA-16 composites with various amount of GO at 77 K. Adsorption isotherms of carbon dioxide (solid) and methane (half left solid) on UTSA-16-GO9.5 (blue diamond), UTSA-16-GO19 (red circle) and UTSA-16-GO28.5 (oliver triangles) at 296 K (b) and 273 K (c). (d) Selectivities of CO_2 over CH_4 predicted for UTSA-16 and its composites by IAST for CO_2 (50%) and CH_4 (50%) at 296 K.

Conclusion

In summary, we have developed an approach to prepare the core−shell nanocomposites, based on MOFs as core armored with controllable grapheme oxide shells. With the assistance of the grapheme oxide shells, the thermal stability and CO_2/CH_4 selectivity of the MOFs have been improved significantly, which demonstrates the GO composites provide a new direction for making practical MOF materials with high performance.

Acknowledgements

This work was financially supported by the National Natural Science Foundation of China (21207018, 21273033 and 21203024) and the Fujian Science and Technology Department (2014J06003). S. X. gratefully

acknowledges the support of the Recruitment Program of Global Young Experts, Program for New Century Excellent Talents in University (NCET-10-0108), and the Award 'MinJiang Scholar Program' in Fujian Province.

References

1 http://european-biogas.eu/2013/12/20/eba-presents-latest-biogas-production-statistics-europe-growth-continuous/

2 Z.-Y. Wang, D.-M. Ren and H. Gao, The Renewable Energy Industrial Development Report 2012, China Economy Press, 2013.

3 Key GHG Data, *United Nations Framework Convention on Climate Change,* Bonn, Germany, 2005.

4 R. S. Haszeldine, *Science*, 2009, **325**, 1647.

5 Y. He, H. Furukawa, C. Wu, M. O'Keeffe, R. Krishna and B. Chen, *Chem. Commun.*, 2013, **49**, 6773.

6 J. Liu, J. Tian, P. K. Thallapally and B. P. Mcgrail, *J. Phys. Chem. C*, 2012, **116**, 9575.

7 K. Munusamy, G. Sethia, D. V. Patil, P. B. S. Rallapalli and R. S. Somani, *Chem. Eng. J.*, 2012, **195-196**, 359.

8 M. Anbia and V. Hoseini, *Chem. Eng. J.*, 2012, **191**, 326.

9 A. Yang, H. Y. Cho, J. Kim, S. T. Yang and W. S. Ahn, *Energy Environ. Sci.*, 2012, **5**, 6465.

10 E. J. García, J. P. S. Mowat, P. A. Wright, J. P. Pellitero, C. Jallut and G. D. Pirngruber, *J. Phys. Chem. C*, 2012, **116**, 26636.

11 T. Remy, S. A. Peter, S. V. Perre, P. Valvekens, D. E. Vos, G. V. Varon and J. F. M. Denayer, *J. Phys. Chem. C*, 2013, **117**, 9301.

12 S. -T. Yang, J. Kim and W.-S. Ahn, *Microporous Mesoporous Mater.*, 2010, **135**, 90.

13 K. S. Walton, M. B. Abney and M. D. Levan, *Microporous Mesoporous Mater.*, 2006, **91**, 78.

14 C. Chen, D.-W. Park and W. -S. Ahn, *Appl. Surf. Sci.*, 2014, **292**, 63.

15 S. García, M. V. Gil, C. F. Martín, J. J. Pis, F. Rubiera and C. Pevida, *Chem. Eng. J.*, 2011, **171**, 549.

16 J. Song, W. Z. Shen, J. G. Wang and W. B. Fan, *Carbon*, 2014, **69**, 255.

17 K. Labus, S. Gryglewicz and J. Machnikowski, *Fuel*, 2014, **118**, 9.

18 M. Auta, N. D. A. Darbis, A. T. M. Din and B. H. Hameed, *Chem. Eng. J.*, 2013, **233**, 80.

19 S. Cavenati; C. A. Grande and A. E. Rodrigues, *J. Chem. Eng. Data*., 2004, **49**, 1095.

20 R. Krishna and J. M. van Baten, *Phys. Chem. Chem. Phys.*, 2011, **13**, 10593.

21 M. R. Hudson, W. L. Queen, J. A. Mason; D. W. Fickel, R. F. Lobo and C. M. Brown, *J. Am. Chem. Soc.*, 2012, **134**, 1970.

22 X. –Z. Luo, X. –J. Jia, J. –H. Deng, J. –L. Zhong, H. –J. Liu, K. –J. Wang and D.-C. Zhong, *J. Am. Chem. Soc.,* 2013, **135**, 11684.

23 R. Dawson, A. I. Cooper and D. J. Adams, *Polym. Int.*, 2013, **62**, 345.

24 W. Lu, J. Sculley, D. Yuan, R. Krishna, Z. Wei and H. -C. Zhou, *Angew. Chem. Int. Ed.*, 2012, **51**, 7480.

25 W. Lu, W. M. Verdegaal, J. Yu, P. B. Balbuena, H. -K. Jeong and H. -C. Zhou, *Energy Environ. Sci.*, 2013, **6**, 3559.

26 W. Lu, J. Sculley, D. -Q. Yuan, R. Krishna and H. -C. Zhou, *J. Phys. Chem. C.*, 2013, **117**, 4057.

27 Y. Xie, T. -T. Wang, X. -H. Liu, K. Zou and W.-Q. Deng, *Nature Commun.*, 2013, **4**, 1960.

28 J. Tian, P. K. Thallapally, S. J. Dalgarno, P. B. McGrail and J. L. Atwood, *Angew. Chem. Int. Ed.,* 2009, **48**, 5492.

29 T. Hasell, J. A. Armstrong, K. E. Jelfs, F. H. Tay, K. M. Thomas, S. G. Kazarian and A. I. Cooper, *Chem. Commun.*, 2013, **49**, 9410.

30 D. M. D'Alessandro, B. Smit and J. R. Long, *Angew. Chem., Int. Ed.*, 2010, **49**, 6058.

31 K. Sumida, D. L. Rogow, J. A. Mason, T. M. McDonald, E. D. Bloch, Z. R. Herm, T. -H. Bae and J. R. Long, *Chem. Rev.*, 2012, **112**, 724.

32 J. -R. Li, Y. Ma, M. C. McCarthy, J. Sculley, J. Yu, H. -K. Jeong, P. B. Balbuena and H. -C. Zhou, *Coord. Chem. Rev.***,** 2011, **255**, 1791.

33 R. Vaidhyanathan, S. S. Iremonger, G. K. H. Shimizu, P. G. Boyd, S. Alavi and T. K Woo, *Science*, 2010, **330**, 650.

34 J.-P. Zhang and X.-M. Chen, *J. Am. Chem. Soc.*, 2009, **131**, 5516.

35 S. Takamizawa, E. Nakata, T. Akatsuka, R. Miyake, Y. Kakizaki, H. Takeuchi, G. Maruta and S. Takeda, *J. Am. Chem. Soc.*, 2010, **132**, 3783.

36 A. R. Millward and O. M. Yaghi, *J. Am. Chem. Soc.*, 2005, **127**, 17998.

37 H. Furukawa, N. Ko, Y. B. Go, N. Aratani, S. B. Choi, E. Choi, A. Ö. Yazaydin, R. Q. Snurr, M. O´Keeffe, J. Kim and O. M. Yaghi, *Science*, 2010, **329**, 424.

38 S. D. Burd, S. Ma, J. A. Perman, B. J. Sikora, R. Q. Snurr, P. K. Thallapally, J. Tian, L. Wojtas and M. J. Zaworotko, *J. Am. Chem. Soc.*, 2012, **134**, 3663.

39 P. Nugent, Y. Belmabkhout, S. D. Burd, A. J. Cairns, R. Luebke, K. Forrest, T. Pham, S. Ma, B. Space, L. Wojtas, M. Eddaoudi and M. J. Zaworotko, *Nature*, 2013, **495**, 80.

40 S. -C. Xiang, Y. -B. He, Z. -J. Zhang, H. Wu, W. Zhou, R. Krishna and B. –L. Chen, *Nature Commun.*, 2012, **3**, 954.

41 Z. Zhang, Z.-Z. Yao, S. Xiang and B. Chen, *Energy Environ. Sci.*, 2014, **7**, 2868.

42 Q.-L. Zhu and Q. Xu, *Chem. Soc. Rev.*, 2014, **43**, 5468.

43 C. Petit and T. J. Bandosz, *Adv. Mater.*, 2009, **21**, 4753.

44 C. Petit and T. J. Bandosz, *Adv. Funct. Mater.*, 2010, **20**, 111.

45 C. Petit and T. J. Bandosz, *Adv. Funct. Mater.*, 2011, **21**, 2108.

46 C. Petit, J. Burress and T. J. Bandosz, *Carbon*, 2011, **49**, 563.

47 C. Petit, B. Levasseur, B. Mendoza and T. J. Bandosz, *Microporous and Mesoporous Mater.*, 2012, **154**, 107.

48 Z. -H. Huang, G. Liu and F. Kang, *ACS Appl. Mater. Interfaces*, 2012, **4**, 4942

49 S. Liu, L. Sun, F. Xu, J. Zhang, C. Jiao, F. Li, Z. Li, S. Wang, Z. Wang, X. Jiang, H. Zhou, L. Yange and C. Schickf, *Energy Environ. Sci.*, 2013, **6**, 818.

50 D. –D. Zu, L. Lu, X. -Q. Liu, D. –Y. Zhang and L. –B. Sun, *J. Phys. Chem. C*, 2014, **118**, 19910.

51 X. Sun, Q. Xia, Z. Zhao, Y. Li and Z. Li, *Chem. Eng. J.*, 2014, **239**, 226.

52 S. -C. Xiang, X.-T. Wu, J. -J. Zhang, R. -B. Fu, S. -M. Hu and X. -D. Zhang, *J. Am. Chem. Soc.*, 2005, **127**, 16352.

53 D. C. Marcano, D. V. Kosynkin, J. M. Berlin, A. Sinitskii, Z. Sun, A. Slesarev, L. B. Alemany, W. Lu and J. M. Tour, *ACS Nano.*, 2010, **4**, 4806.

54 I. P. O'koye, M. Benham and K. M. Thomas, *Langmuir*, 1997, **13**, 4054.

55 S. -C. Xiang, Z. -J. Zhang, C. -G. Zhao, K. Hong, X. Zhao, D. -R. Ding, M. -H. Xie, C. -D. Wu, M. C. Das, R. Gill, K. M. Thomas and B. Chen, *Nat. Commun.*, 2011, **2**, 204.

56 A. L. Myers and J. M. Prausnitz, *AIChE J.*, 1965, **11**, 121.

57 S. Stankovich, D. A. Dikin, R. D. Piner, K. A. Kohlhaas, A. Kleinhammes, Y. Jia, Y. Wu, S. T. Nguyen and R. S. Ruoff, *Carbon*, 2007, **45**, 1558.

58 P. Goli, H. Ning, X. Li, C. Y. Lu, K. S. Novoselov and A. A. Balandin, *Nano Lett*., 2014, **14**, 1497−1503.

59 P. Chowdhury, S. Mekala, F. Dreisbach, and S. Gumma, *Microporous Mesoporous Mater.* 2012, **152**, 246.

60 Q. Yan, Y. Lin, C. Kong and L. Chen, *Chem. Commun.*, 2013, 49, 6 873 - 6875.